



Synthesis, crystal structure, electronic structure, bonding, photoluminescence and spectroscopic property investigations of a mononuclear 1,10-phenanthroline and 5-bromo-salicylate ternary indium(III) complex

Yi-Ping Tong^{a,b,*}, Yan-Wen Lin^c

^aInstitute of Inorganic Chemistry, Hanshan Normal University, Chaozhou 521041, China

^bDepartment of Chemistry, Hanshan Normal University, Chaozhou 521041, China

^cDepartment of Biology, Hanshan Normal University, Chaozhou 521041, China

ARTICLE INFO

Article history:

Received 7 April 2009

Received in revised form 30 June 2009

Accepted 2 July 2009

Available online 9 July 2009

Keywords:

Indium complex

5-Bromo-salicylic acid

Crystal structure

TDDFT level

Mixed-ligand

Partial density of states (PDOSs)

ABSTRACT

The synthesis, X-ray structure, electronic structure, bonding, photoluminescence, spectroscopic property and characterization of an indium(III) complex, $[\text{In}(\text{Hbsac})_3(\text{phen})]$ (**1**) (H_2bsac = 5-bromo-salicylic acid, and phen = 1,10-phenanthroline) are presented. Complex **1** is octacoordinate and carboxylate chelating, being novel and rarely reported for main group complexes. The electronic structure, bonding and the charge transfer properties of light excitation and light emission are discussed in detail using first-principles theory, including partial density of states (PDOSs), crystal orbital overlap population (COOP), the density functional theory (DFT/TDDFT) analysis schemes. The charge transfer is mainly $\pi \rightarrow \pi^*$ intraligand charge transfer transition (ILCT) for excitation, and $\pi \rightarrow \pi^*$ ligand-to-ligand charge transfer transition (LL'CT) for emission in nature.

© 2009 Elsevier B.V. All rights reserved.

1. Introduction

Indium complexes with chelating ligands are an important class of coordination complex, finding interesting coordination structures in coordination chemistry, such as unusual coordination modes [1–5], and potential applications in material sciences, such as light emitters in photoluminescence and/or electroluminescence [6–11].

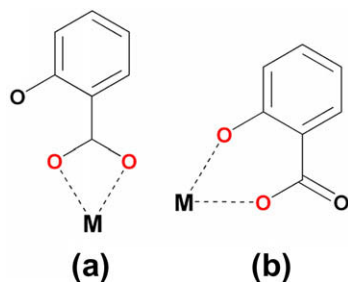
Though the strong propensity of group 13 metals, in general, to form stable six-coordinative complexes is well-known [8,12,13], some octacoordinate indium(III) complexes with chelating ligands have been found and characterized structurally over the past years [1,5]. To the best of our knowledge, such octacoordinate metal complexes are rarely reported for other main group metals, thus, such indium(III) compounds offer potential opportunities either for studies of rare bonding modes (octacoordinate number or higher) between main group metal center and chelating ligands in coordination chemistry [1,5] or for seeking for new functional organometal materials, such as light-emitting materials, and for interesting aspects of physical and chemical properties for these

new class of materials, such as behavior in photophysics and photochemistry, and properties in spectroscopy [1,5,14].

Salicylic acid and its derivatives are a class of heterodifunctional chelating ligands capable of bonding to a range of metal centers as either a monoanion or a dianion [15–20], and are capable of coordinating in a range of bonding modes [21–25]. Scheme 1 represents two possible chelating coordination modes for salicylic acid-derived ligands, i.e. the carboxylate chelating mode and the carboxylate–phenolate chelating mode; in general, the former is favoured for the formation of complexes with higher coordinative number owing to relatively less steric hindrance and contrarily, the latter is favoured for the formation of complexes with lower coordinative number owing to the relatively larger steric effect. Therefore, octacoordinate, and carboxylate chelating organometallic complexes with salicylic acid-derived ligands may be reasonably possible, and indeed, some octacoordinate, and carboxylate chelating indium(III) analogues with other carboxylic acid ligands have been crystallographically verified recently [1,5]. However, up to now, no such complexes with salicylic acid derivatives have been found. In this paper, we report the synthesis, crystal structure, electronic structure, bonding, photoluminescence and spectroscopic property investigations on a ternary mononuclear indium(III) complex with 5-bromo-salicylic acids (H_2bsac = 5-bromo-salicylic acid) and 1,10-phenanthroline (phen = 1,10-phenanthroline), namely, $[\text{In}(\text{Hbsac})_3(\text{phen})]$ (**1**), together with

* Corresponding author. Address: Institute of Inorganic Chemistry, Hanshan Normal University, Chaozhou 521041, China. Tel.: +86 768 3692891; fax: +86 768 2525151.

E-mail address: typ2469@163.com (Y.-P. Tong).



Scheme 1. Two types of chelating coordination modes: (a) carboxylate chelating and (b) carboxylate-phenolate chelating.

density functional theory (DFT) and time-dependent density functional theory (TDDFT) studies of this compound.

2. Experimental

2.1. General

All the reagents and solvents employed were commercially available and used as received without further purification. The C, H and N micro-analyses were carried out on an Elementar Vario El elemental analyzer. The FT-IR spectra were recorded using a Nicolet magna-550(II) spectrometer in the KBr pellets in the range 4000–400 cm^{-1} . ^1H NMR spectra were recorded with a Bruker Biospin AVANCE 400 MHz spectrometer. The UV-Vis spectra were recorded on a Varian Cary-100 spectrometer. The steady-state fluorescent spectra were determined with a SHIMADZU Instrument RF5301 fluorescence spectrophotometer. The fluorescence lifetime was determined with an Edinburgh Instrument FLS920 fluorescence spectrophotometer using a H_2 gas lamp as the light source. The ESI-MS was carried out on a high-resolution Finnigan MAT LCQ mass spectrometer.

2.2. Preparation of **1**

The complex was prepared by an electrochemical method. The cell consisted of indium wire as the anode and a platinum wire as the cathode. H_2bsac (0.042 g, 0.2 mmol) and coligand phen (0.020 g, 0.1 mmol) were dissolved in ethanol (60 mL) and a small amount of tetra-*n*-butylammonium perchlorate was added to the solution as a supporting electrolyte. A 30 V voltage was applied to the cell for 6 h to allowed sufficient current flow for smooth dissolution of the indium metal. The cell can be summarized as $\text{In}(+)/\text{ethanol} + \text{H}_2\text{bsac} + \text{phen}/\text{Pt}(-)$. The resultant solution was allowed to stand for ca. four months, a colourless crystal of **1** was obtained in approximate 70% yield based on H_2bsac . *Anal. Calc.* for $\text{C}_{33}\text{H}_{20}\text{Br}_3\text{InN}_2\text{O}_9$ (943.05): C, 42.03; H, 2.14; N, 2.97. Found: C, 42.09; H, 2.21; N, 3.10%. *m/z* (ESI) 942 $\{[\text{In}(\text{Hbsac})_3(\text{phen})]^{-}\}^-$. ^1H NMR (DMSO- d_6 , 400 MHz): 12.75 (s, 3 H), 9.18 (d, $J = 7.63$ Hz, 1 H), 8.47 (m, 2 H), 8.40 (m, 2 H), 7.86 (m, 4 H), 7.54 (d, $J = 5.2$ Hz, 3 H), 6.84 (d, $J = 5.6$ Hz, 3 H). FT-IR (KBr, cm^{-1}): 3130 m, 1589 m, 1466 m, 1433 w, 1385 s, 1248 w, 1146 w, 1106 w, 871 w, 851 w, 825 m, 723 m, 628 w, 532 w, 472 w, 457 w.

2.3. DFT and TDDFT calculations

The geometric optimization for **1** was performed on a Dell precision 490 computer using experimental geometry as input, employing the GAUSSIAN98 suite of programs [26], at spin restricted DFT wavefunctions (B3LYP) level [27,28], i.e. the Becke three-parameter exchange functional in combination with the LYP correlation functional of Lee, Yang and Parr with 6-311G** basis set for C,

H, N and O atoms, and effective core potentials basis set LanL2DZ for In and Br atoms. The optimized calculation was confirmed to be local minima by performing harmonic vibration frequency analyses (no imaginary frequency found). No symmetry constraints were applied and only the default convergence criteria were undertaken during optimization.

Based on the optimized geometries, TDDFT calculations were performed at the same B3LYP level, and with the same basis sets as in DFT calculation for C, H, N, O, Br and In atoms to calculate the vertical electron transition energies. The electron density diagrams of molecular orbitals were obtained with the MOLDEN 3.5 graphics program [29].

2.4. Crystal structure determination and refinements

Diffraction intensities for **1** were collected at 293 K on a Bruker Smart Apex CCD diffractometer (Mo $K\alpha$, $\lambda = 0.71073$ Å). Absorption corrections were applied by using SADABS [30]. The structures were solved with direct methods and refined with full-matrix least-squares technique using SHELXTL program package [31]. The organic hydrogen atoms were generated in ideal positions. Anisotropic thermal parameters were applied to all non-hydrogen atoms. Experimental details of the X-ray analyses are provided in Table 1. Selected bond lengths and angles are listed in Table 2.

3. Results and discussion

3.1. Crystal structure of **1**

Fig. 1 shows the molecular structure of **1** together with the labeling scheme used. Selected geometric parameters are listed in Table 2. Complex **1** is a monomer with InN_2O_6 core in which the six chelating carboxylate oxygen atoms from three Hbsac^- ligands and two nitrogen atoms from one phen ligand, overall yielding an octacoordinate geometry. A pair of Hbsac^- ligands (L1 and L3) are located at approximately opposite sites to each other

Table 1
Crystal data and structure refinement for **1**.

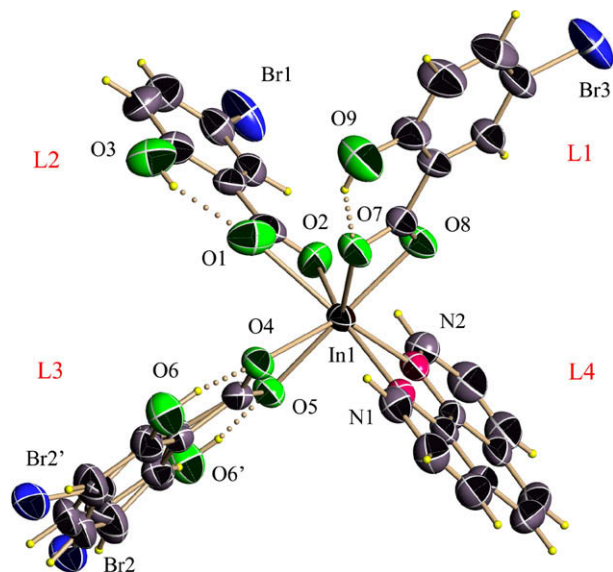
Compound	1
Empirical formula	$\text{C}_{33}\text{H}_{20}\text{Br}_3\text{InN}_2\text{O}_9$
Formula weight	943.06
<i>T</i> (K)	293(2)
Crystal system	triclinic
Space group	$P\bar{1}$ (no. 2)
<i>a</i> (Å)	12.0012(8)
<i>b</i> (Å)	12.6354(8)
<i>c</i> (Å)	12.9974(8)
α (°)	74.1990(10)
β (°)	85.1150(10)
γ (°)	61.9000(10)
<i>V</i> (Å ³)	1670.75(18)
<i>Z</i>	2
μ (mm ⁻¹)	4.352
Crystal size (mm)	0.45 × 0.29 × 0.25
θ Range for data collection (°)	1.89–27.00
Index ranges	$-15 \leq h \leq 15$, $-16 \leq k \leq 16$, $-15 \leq l \leq 16$
Total reflections	14 056
Unique reflections (R_{int})	7153 [0.0281]
Completeness to θ_{max}	97.9
Observed data/restraints/parameters	7153/3/436
<i>S</i> on F^2	1.019
R_1^a ($I > 2\sigma(I)$)	0.0483
wR_2^b (all data)	0.1286
Largest difference in peak and hole (e Å ⁻³)	1.383 and -1.063

^a $R_1 = \sum ||F_o| - |F_c|| / \sum |F_o|$.

^b $wR_2 = [\sum w(F_o^2 - F_c^2)^2 / \sum w(F_o^2)^2]^{1/2}$.

Table 2Selected experimental/calculated bond lengths and angles (Å, °) for **1**.

In(1)–O(1)	2.437(5)/2.201	In(1)–N(1)	2.301(4)/2.361
In(1)–O(2)	2.230(5)/2.325	In(1)–N(2)	2.303(4)/2.392
In(1)–O(4)	2.380(4)/2.373	Br(1)–C(16)	1.897(6)/1.959
In(1)–O(5)	2.214(4)/2.185	Br(2)–C(23)	1.886(4)/1.959
In(1)–O(7)	2.430(4)/2.374	Br(2')–C(23')	1.885(7)/1.959
In(1)–O(8)	2.201(4)/2.185	Br(3)–C(30)	1.885(6)/1.959
O(8)–In(1)–O(5)	168.18(13)/163.7	O(8)–In(1)–O(1)	94.71(15)/94.7
O(8)–In(1)–O(2)	84.67(16)/86.9	O(4)–In(1)–O(7)	79.48(12)/80.6
O(5)–In(1)–O(2)	86.13(15)/87.0	O(2)–In(1)–O(7)	114.50(16)/124.1
O(8)–In(1)–N(1)	91.74(15)/88.6	O(5)–In(1)–O(1)	86.02(15)/94.7
O(5)–In(1)–N(1)	93.22(14)/88.7	O(2)–In(1)–O(1)	54.84(16)/57.5
O(2)–In(1)–N(1)	153.73(17)/148.3	O(4)–In(1)–O(1)	76.53(15)/82.2
O(8)–In(1)–N(2)	84.63(14)/82.0	O(7)–In(1)–O(1)	76.93(14)/82.2
O(5)–In(1)–N(2)	86.71(14)/82.0	N(1)–In(1)–O(7)	83.93(14)/78.1
O(2)–In(1)–N(2)	81.72(17)/78.7	N(2)–In(1)–O(7)	132.89(14)/128.1
O(8)–In(1)–O(4)	134.98(13)/137.5	N(1)–In(1)–O(1)	151.38(15)/154.2
O(5)–In(1)–O(4)	56.65(13)/57.1	N(2)–In(1)–O(1)	136.32(16)/136.2
O(2)–In(1)–O(4)	120.98(15)/124.1	N(1)–In(1)–N(2)	72.03(15)/69.7
O(8)–In(1)–O(7)	55.63(13)/57.1	N(1)–In(1)–O(4)	79.22(14)/78.1
O(5)–In(1)–O(7)	135.64(12)/137.5	N(2)–In(1)–O(4)	131.67(14)/128.1

**Fig. 1.** ORTEP drawing of **1** with 50% probability thermal ellipsoids. The dash lines represent intramolecular hydrogen bonding (O–H...O) interactions.

around the central indium(III), as reflected by a large angle of O(5)–In(1)–O(8) of 168.18(13)°, and similarly, the other pair of ligands (L2: another one Hbsac[−] and L4: phen ligand) surround In(III) center on approximately opposite vertices as both the O(1)–In(1)–N(1) and O(2)–In(1)–N(1) angles are as large as 151.38(15) and 153.73(17)°, respectively. Furthermore, in InN₂O₆ core, both the In1, O4, O5, O7 and O8 atoms and the In1, O1, O2, N1 and N2 atoms are approximately coplanar, as the mean deviation of these atoms are as little as 0.06 and 0.04 Å, respectively. These planes are essentially perpendicular with a corresponding dihedral angle of ca. 89.7°. Thus two pairs of chelating ligands (L1 and L3, L2 and L4) may be considered to be approximately located on two mutual perpendicular planes, furnishing two orthogonal square-planar arrangements around the same In(III) center. Both square-planar geometries are highly distorted as indicated by the smaller bite angles of the Hbsac[−] and phen ligands (Table 2). All the In–O and In–N lengths are typical and similar to other octacoordinate indium(III) complexes [1], and the two In–N bond lengths are identical within 0.002 Å for phen ligand, but for In–O dimensions, one In–O bond length is ca. 0.17–0.23 Å shorter than another one for each Hbsac[−] ligand, indicating that one carboxylate oxygen atom is obviously much more strongly bonded to the In(III) atom than the other in each Hbsac[−] ligand, while two In–N interactions are almost identical for phen ligand.

For L3 moiety, the crystallographically determined structure exhibits disorder owing to a rotation about the bond linking the carboxylate and phenol ring. The final conformation occupancy factor was refined to almost 0.93, indicating one conformation (labeling O6...Br2, Fig. 1) is predominant over another one (labeling O6'...Br2') (Fig. 1).

Strong intermolecular π – π stacking interactions between phen (L4) and Hbsac[−] (L2) ligand rings of adjacent **1** molecules are observed in a head-to-tail way in the lattice with an inter-plane distance of ca. 3.37 Å (Fig. 2). Moreover the intramolecular hydrogen bonding between Hbsac[−] O–H groups and carboxylate O atoms (O3...O1 2.617(7), O6...O4 2.590(6), O6'...O5 2.62(6) and O9...O7 2.616(6) Å) are also present (Fig. 1); Both the π – π stacking interactions and the hydrogen bonding interactions contribute critically to the stability of the real solid.

3.2. Ground state electronic structure

The optimized geometry parameters for **1** are given in Table 2. The optimized bond distances and angles agree well with the

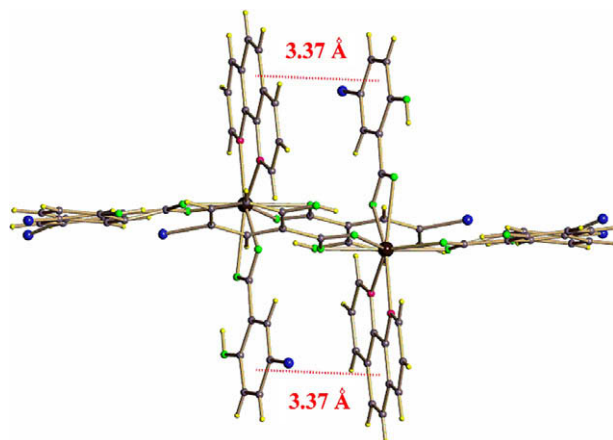
experimental values. The calculated molecular orbital energy level diagrams are presented in Fig. 3.

For **1**, the HOMO and LUMO orbitals are predominantly π bonding orbital of L2 ligand (Hbsac[−]) and π^* antibonding orbital of L4 ligand (phen), respectively with little contribution from In(III). The high-lying occupied orbitals (HOMO–1 to HOMO–15) are all mainly π bonding orbitals of L1 (Hbsac[−]), L2 (Hbsac[−]), L3 (Hbsac[−]) and L4 (phen) (Fig. 3), while the orbitals with In character are far below these orbitals in energy.

The low-lying unoccupied orbitals just above the LUMO orbital in energy (LUMO+1 to LUMO+9) are all ligand π^* antibonding orbitals in character (LUMO+1, LUMO+2, and LUMO+6: π^* of L4 (phen); LUMO+5: π^* of L2 (Hbsac[−], 87%); other: π^* of L1 (Hbsac[−]) + L3 (Hbsac[−])). No orbitals with obvious In character can be found in these orbitals, thus both occupied and unoccupied frontier orbitals are ligand-centered, and these orbitals are responsible for the light excitation process (mentioned below).

3.3. Metal–ligand bonding

Density of states (DOSs) or partial density of states (PDOSs), in combination with molecular orbital, especially frontier molecular

**Fig. 2.** Perspective view of π – π stacking interactions in **1**.

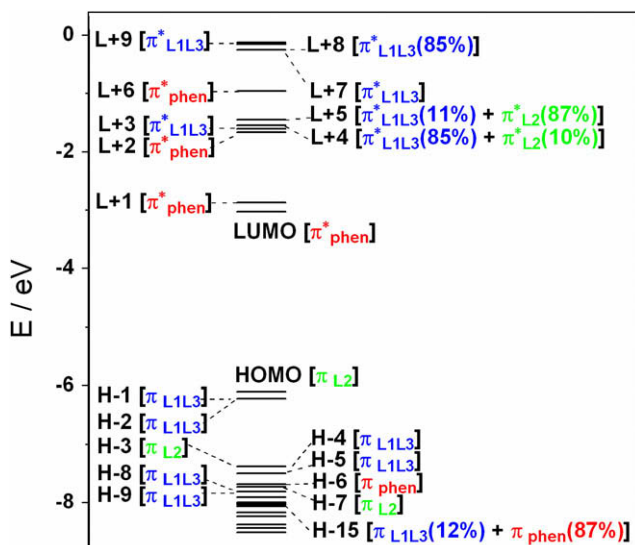


Fig. 3. The frontier molecular orbital energy level diagram of **1**.

orbital, gives the overall electronic structure of a system. Crystal orbital overlap population (COOP) analysis helps in studying the detailed bonding between a group of atoms and the other atoms in a system. The PDOSs and COOP of **1** are plotted in Figs. 4 and 5, respectively. The bonding in **1** was analyzed qualitatively using these first-principles methods. The analysis revealed the clear band gap and the fact that the states in the region of energy (-15 – 0 eV) are mainly constructed from the ligands (L1–L4) orbitals and the contributions from In center are much less and somewhat negligible (Fig. 4). These ligand orbitals are not fully localized but rather mixed with one another, which is in agreement with the analyses of molecular orbital (above). Slight metal–ligand antibonding interactions are observed just near the HOMO level, and clear antibonding interactions are also present between In center and L1 and L3 ligands near the LUMO level, however the In–L2 metal–ligand interaction is non-bonding and the In–L4 interaction is bonding in vicinity of LUMO level (Fig. 5). All the metal–ligand interactions above LUMO level in energy are antibonding in nature and are unfilled. Contrarily, all the metal–ligand interaction below HOMO level in energy (-15 – 7 eV) are all basically bonding in nature and are filled, though two distinct regions of the In–L4 antibonding interaction and one distinct region of the In–(L1,L3) antibonding interactions are seen at this energy region, respectively (Fig. 5).

The PDOSs plot therefore suggests a small degree of covalency of the metal–ligand bonds. This is in agreement with the electronic population on the In atom, the net charges calculated by Mulliken population analysis scheme (MPA) being 1.5 positive charge for **1**. This electron transfer is mainly into the 5s orbital on the In atom. Taking the analysis of the orbital interactions and the atomic charges together it is plausible to propose the qualitative bonding picture, which includes the mainly ionic interaction between the central In atom and the ligands.

3.4. Electronic spectrum and properties

The absorption spectrum of **1** in chloroform is recorded for comparison with the calculated spectrum based on singlet excited states. Only the excited states that arise from singlet–singlet transitions were correlated with the UV–Vis spectrum. The experimental UV–Vis spectrum of **1** shows two low-lying absorption bands at 289 and 310 nm with ϵ roughly $12\,359$ and $1748\text{ M}^{-1}\text{ cm}^{-1}$, respectively (Table 3).

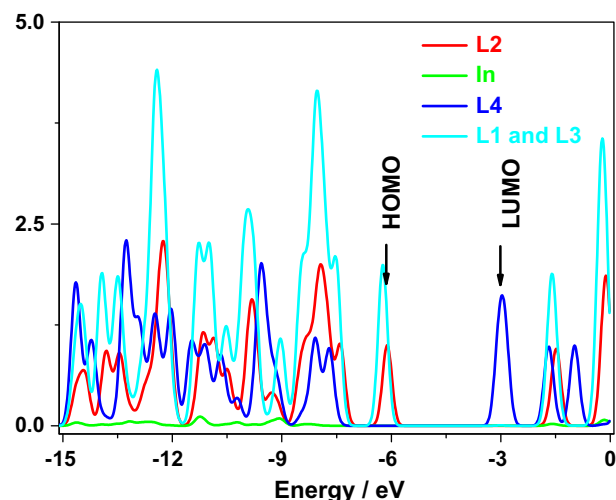


Fig. 4. Partial density of states (PDOSs) for **1**.

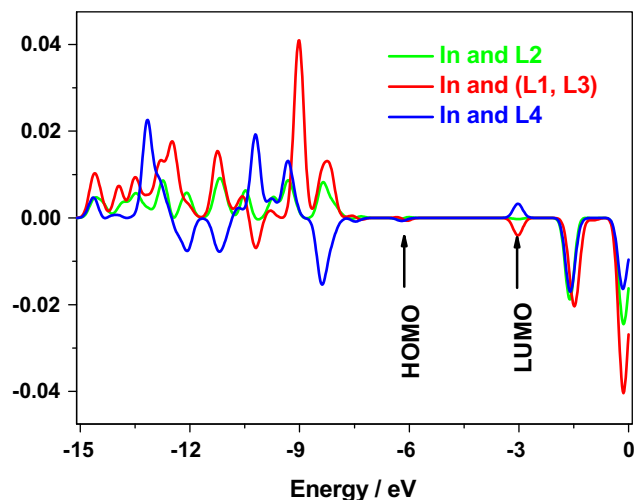


Fig. 5. The crystal orbital overlap population (COOP) for the bandstructure of **1**.

The primary feature of the TDDFT calculated absorption bands of **1** (Table 3) shows two moderately-to-strongly intense low-energy absorptions at 303 and 314 nm with oscillator strength 0.0883 and 0.0113, respectively. The oscillator strength variations for the two bands are in very agreement with those of the molar absorptivity of the two experimental bands, thus the two low-energy absorption bands (303 and 314 nm) can be readily associated with the experimental low-lying absorption bands in UV–Vis spectrum (289 and 310 nm), with the difference between the calculated peaks compared to the experimental ones likely due to solvent effects. In fact, our TDDFT calculation has also predicted the lowest energy excited state and ground state (ES-GS) separation and this lowest energy absorption band is 448 nm in a lower energy range, and has a much weaker oscillator strength predicted (0.0003) than for those mentioned above (Table 3). This absorption may be very weak in absorption intensity, and was not observed in the experimental UV–Vis spectrum for **1**.

Only the most significant transitions associated with each absorption band are listed in Table 3. For example, for 448 nm absorption band, many transitions are calculated. One transition is listed in Table 3 (HOMO \rightarrow LUMO (98%)) as only its percentage orbital transition composition is over 5%. If multiple transitions

Table 3Experimental and calculated UV-Vis absorption bands, oscillator strengths, transition configurations and transition properties of **1**.

Calculated/experimental (nm)	f/ϵ ($M^{-1} cm^{-1}$)	Transition configuration	Character
448	0.0003	HOMO \rightarrow LUMO (98%)	$\pi \rightarrow \pi^*$ (LL'CT)
314/310	0.0113/1748	HOMO-6 \rightarrow LUMO (44%) HOMO-4 \rightarrow LUMO (22%) HOMO-3 \rightarrow LUMO (18%)	$\pi \rightarrow \pi^*$ (ILCT) $\pi \rightarrow \pi^*$ (LL'CT) $\pi \rightarrow \pi^*$ (LL'CT)
303/289	0.0883/12 359	HOMO-15 \rightarrow LUMO+1 (9%) HOMO-2 \rightarrow LUMO+3 (37%) HOMO \rightarrow LUMO+2 (23%) HOMO-1 \rightarrow LUMO+4 (19%) HOMO-1 \rightarrow LUMO+2 (7%)	$\pi \rightarrow \pi^*$ (ILCT) $\pi \rightarrow \pi^*$ (ILCT) $\pi \rightarrow \pi^*$ (LL'CT) $\pi \rightarrow \pi^*$ (ILCT) $\pi \rightarrow \pi^*$ (LL'CT)

have percentage orbital transition composition with absolute values over 5%, they are all listed, for example, the 314 nm absorption band in Table 2 (HOMO-6 \rightarrow LUMO (44%), HOMO-4 \rightarrow LUMO (22%), HOMO-3 \rightarrow LUMO (18%) and HOMO-15 \rightarrow LUMO+1 (9%)) and the 303 nm absorption band (HOMO-2 \rightarrow LUMO+3 (37%), HOMO \rightarrow LUMO+2 (23%), HOMO-1 \rightarrow LUMO+4 (19%) and HOMO-1 \rightarrow LUMO+2 (7%)).

According to our TDDFT calculations, the low-energy 314 nm absorption band (oscillator strength 0.0113) mainly arises from four transitions with percentage orbital transition composition over 5% (Table 3). Owing to being the π bonding orbital of ligand L4 (phen) for HOMO-6 and HOMO-15, the π bonding orbitals of ligand L1L3 (Hbsac⁻) and of ligand L2 (Hbsac⁻) for HOMO-4 and

HOMO-3, respectively, and the π^* antibonding orbital of L4 (phen) for LUMO and LUMO+1 in character (Figs. 3 and 6), thus the 314 nm absorption band is mainly labeled as a phen(L4)-centered intraligand charge transfer (ILCT) [32,33], but mixed with Hbsac⁻(L1L3 and L2)-to-phen(L4) ligand-to-ligand charge transfer (LL'CT) transition with $\pi \rightarrow \pi^*$ nature (Table 3). Similarly, the 303 nm absorption band (oscillator strength 0.0883) can mainly ascribed as a Hbsac⁻(L1L3)-centered intraligand charge transfer (ILCT) [32,33], but mixed with Hbsac⁻(L2)-to-phen(L4) ligand-to-ligand charge transfer (LL'CT) transition with $\pi \rightarrow \pi^*$ nature (Table 3).

3.5. Luminescent spectrum and properties

Complex **1** is photoluminescent in chloroform. The emission maximum for **1** is 457 nm with corresponding excitation wavelength 324 nm in chloroform (Fig. 7). Similar to those of other In(III) metal complexes [8], the lifetime of **1** is ca. 2.58 ns in trichloromethane at room temperature.

According to the TDDFT calculation and molecular orbital analyses, the transitions in lowest excited state ground state (ES-GS) separation of **1** is mainly associated with the transitions from the corresponding HOMO to LUMO (percentage orbital transition composition up to 98%), in which the HOMO is mainly the π bonding orbital of Hbsac⁻(L2), while the LUMO is the π^* antibonding orbital of phen(L4); thus, according to the energy-gap law for radiationless deactivation [34–42], the photoluminescence here should be described as a ligand-to-ligand charge transfer transition with $\pi \rightarrow \pi^*$ nature (LL'CT) [43].

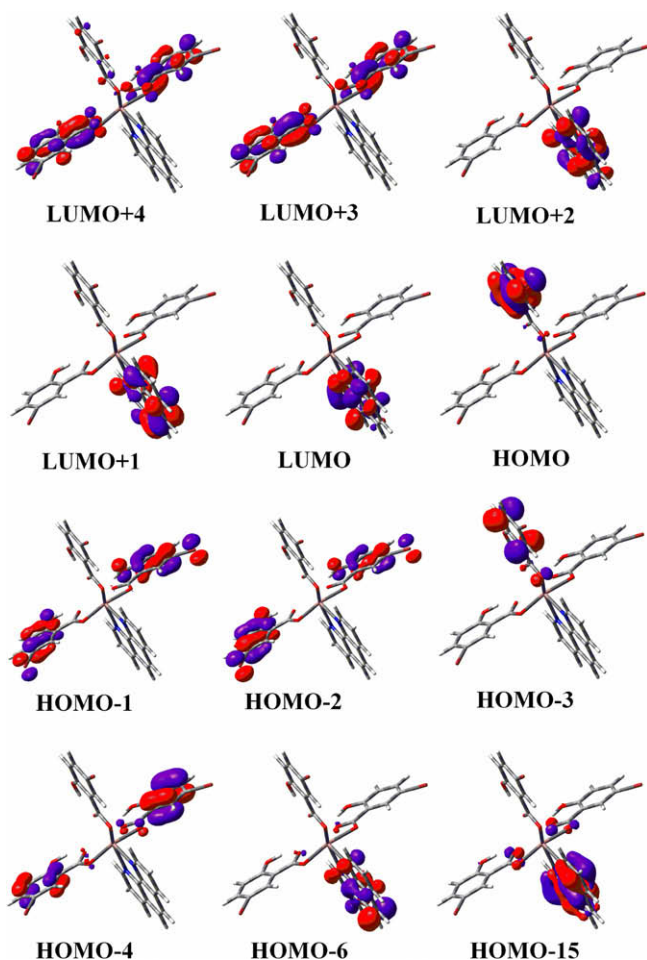


Fig. 6. Contour surfaces of the frontier molecular orbitals most involved in the calculated excitations of UV-Vis spectra of **1**.

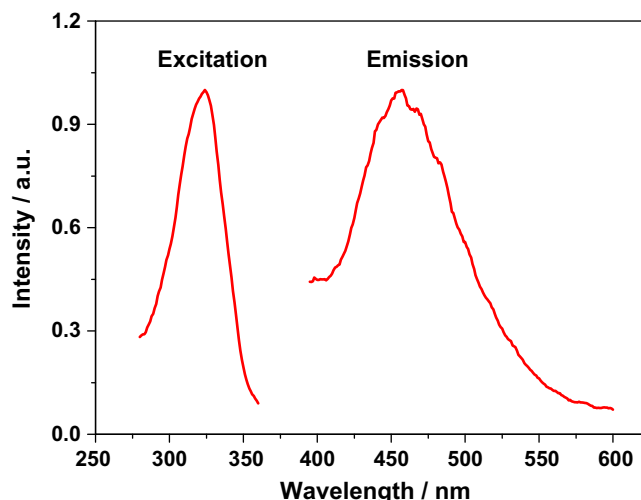


Fig. 7. The excitation and emission spectra for **1** in chloroform.

4. Conclusions

A mononuclear, octacoordinate, carboxylate chelating ternary indium(III) complex with 5-bromo-salicylic acid and 1,10-phenanthroline, $[\text{In}(\text{Hbsac})_3(\text{phen})]$ (**1**) has been synthesized and characterized crystallographically. Complex **1** crystallizes in the triclinic system, space group $P\bar{1}$ (no. 2), with the unit cell dimensions $a = 12.0012(8)$ Å, $b = 12.6354(8)$ Å, $c = 12.9974(8)$ Å, $\alpha = 74.1990(10)^\circ$, $\beta = 85.1150(10)^\circ$, $\gamma = 61.9000(10)^\circ$ and $Z = 2$. Such octacoordinate geometry in **1** is novel and rarely reported so far for main group metal complexes. The electronic structure and bonding property of metal–ligand interactions are discussed in detail using first-principles theory with partial density of states (PDOSs) and crystal orbital overlap population (COOP) analysis schemes. DFT- and TDDFT-based theoretical calculation results show considerable agreement with experimental ones. **1** exhibits typical $\pi \rightarrow \pi^*$ ligand-centered, intraligand charge transfer nature (ILCT), but mixed with ligand-to-ligand charge transfer transitions (LL'CT) for the low-lying UV–Vis absorption bands. The emissive state of **1** is assigned as a singlet $\pi \rightarrow \pi^*$ ligand-to-ligand charge transfer transition (LL'CT).

Acknowledgments

This work was supported by the Natural Science Foundation of Department of Education of Guangdong Province of China and the Natural Science Foundation of Guangdong Province of China (Grant No. 06301028).

Appendix A. Supplementary material

CCDC 641727 contains the supplementary crystallographic data for **1**. These data can be obtained free of charge from The Cambridge Crystallographic Data Centre via www.ccdc.cam.ac.uk/data_request/cif. Supplementary data associated with this article can be found, in the online version, at [doi:10.1016/j.ica.2009.07.005](https://doi.org/10.1016/j.ica.2009.07.005).

References

- [1] B. Gómez-Lor, E. Gutiérrez-Puebla, M. Iglesias, M.A. Monge, C. Ruiz-Valero, N. Snejko, *Chem. Mater.* 17 (2005) 2568.
- [2] Z. Lin, L. Chen, F. Jiang, M. Hong, *Inorg. Chem. Commun.* 8 (2005) 199.
- [3] M.K. Pal, N.P. Kushwah, A.P. Wadawale, V.S. Sagoria, V.K. Jain, E.R.T. Tiekink, *J. Organomet. Chem.* 692 (2007) 4237.
- [4] Z. Tian, L. Wang, T. Song, Y. Wang, L. Huang, L. Zhang, S. Shi, *J. Solid State Chem.* 181 (2008) 842.
- [5] J. Sun, L. Weng, Y. Zhou, J. Chen, Z. Chen, Z. Liu, D. Zhao, *Angew. Chem., Int. Ed. Engl.* 41 (2002) 4471.
- [6] M. Durmuş, T. Nyokong, *Polyhedron* 26 (2007) 3323.
- [7] V. Chauke, M. Durmuş, T. Nyokong, *J. Photochem. Photobiol. A: Chem.* 192 (2007) 179.
- [8] Y.-P. Tong, S.-L. Zheng, X.-M. Chen, *Aust. J. Chem.* 59 (2006) 653.
- [9] Y. Shen, X. Wang, S. Xu, H. Li, *Curr. Appl. Phys.* 7 (2007) 96.
- [10] Y. Chen, Y. Araki, D. Dini, Y. Liu, O. Ito, M. Fujitsuka, *Mater. Chem. Phys.* 98 (2006) 212.
- [11] M. Ghedini, M.L. Deda, I.A. Grisolia, *Synth. Met.* 138 (2003) 189.
- [12] S.-G. Liu, J.-L. Zuo, Y.-Z. Li, X.-Z. You, *J. Mol. Struct.* 705 (2004) 153.
- [13] J. Romero, M.L. Durán, A. Rodríguez, J.A. García-Vázquez, A. Sousa, D.J. Rose, J. Zubieta, *Inorg. Chim. Acta* 274 (1998) 131.
- [14] M.T. Andras, A.F. Hepp, S.A. Duraj, E.B. Clark, D.A. Scheiman, P.E. Fanwick, D.G. Hehemann, *Inorg. Chem.* 32 (1993) 4150.
- [15] J.-P. Costes, J.M. Clemente-Juan, F. Dahan, F. Nicodeme, M. Verelst, *Angew. Chem., Int. Ed. Engl.* 41 (2002) 323.
- [16] L.-G. Zhu, S. Kitagawa, H. Miyasaka, H.-C. Chang, *Inorg. Chim. Acta* 355 (2003) 121.
- [17] J.-H. Yan, W. Li, S.-L. Zheng, Z.-L. Huang, X.-M. Chen, *Aust. J. Chem.* 56 (2003) 1175.
- [18] N.L. Rosi, J. Kim, M. Eddaoudi, B. Chen, M. O'Keeffe, O.M. Yaghi, *J. Am. Chem. Soc.* 127 (2005) 1504.
- [19] J.H. Thurston, A. Kumar, C. Hofmann, K.H. Whitmire, *Inorg. Chem.* 43 (2004) 8427.
- [20] C. Litos, A. Terzis, C. Raptopoulou, A. Rontoyianni, A. Karaliota, *Polyhedron* 25 (2006) 1337.
- [21] J.H. Thurston, T.O. Ely, D. Trahan, K.H. Whitmire, *Chem. Mater.* 15 (2003) 4407.
- [22] S.-Y. Yang, L.-S. Long, R.-B. Huang, L.-S. Zheng, S.W. Ng, *Inorg. Chim. Acta* 358 (2005) 1882.
- [23] X.-M. Zhang, R.-Q. Fang, H.-S. Wu, *CrystEngComm* 7 (2005) 96.
- [24] W.-G. Wang, J. Zhang, L.-J. Song, Z.-F. Ju, *Inorg. Chem. Commun.* 7 (2004) 858.
- [25] S. Zang, Y. Su, Y. Li, Z. Ni, Q. Meng, *Inorg. Chem.* 45 (2006) 174.
- [26] M.J. Frisch, G.W. Trucks, H.B. Schlegel, G.E. Scuseria, M.A. Robb, J.R. Cheeseman, V.G. Zakrzewski, J.A. Montgomery, R.E. Stratmann, J.C. Burant, S. Dapprich, J.M. Millam, A.D. Daniels, K.N. Kudin, M.C. Strain, O. Farkas, J. Tomasi, V. Barone, M. Cossi, R. Cammi, B. Mennucci, C. Pomelli, C. Adamo, S. Clivord, J. Ochterski, G.A. Petersson, P.Y. Ayala, Q. Cui, K. Morokuma, D.K. Malick, A.D. Rabuck, K. Raghavachari, J.B. Foresman, J. Cioslowski, J.V. Ortiz, B.B. Stefanov, G. Liu, A. Liashenko, P. Piskorz, I. Komaromi, R. Gomperts, R.L. Martin, D.J. Fox, T. Keith, M.A. Al-Laham, C.Y. Peng, A. Nanayakkara, C. Gonzalez, M. Challacombe, P.M.W. Gill, B.G. Johnson, W. Chen, M.W. Wong, J.L. Andres, M. Head-Gordon, E.S. Replogle, J.A. Pople, *GAUSSIAN 98*, Revision A9, Gaussian Inc., Pittsburgh, PA, 1998.
- [27] A.D. Becke, *J. Chem. Phys.* 98 (1993) 5648.
- [28] C. Lee, W. Yang, R.G. Parr, *Phys. Rev. B* 37 (1988) 785.
- [29] G. Schaftenaar, *MOLDEN*, Version 3.5, CAOS/CAMM Center Nijmegen, Toernooiveld, Nijmegen, The Netherlands, 1999.
- [30] R. Blessing, *Acta Crystallogr., Sect. A* 51 (1995) 33.
- [31] G.M. Sheldrick, *SHELXTL 6.10*, Bruker Analytical Instrumentation, Madison, Wisconsin, USA, 2000.
- [32] Y.-P. Tong, S.-L. Zheng, X.-M. Chen, *J. Mol. Struct.* 826 (2007) 104.
- [33] Y.-P. Tong, S.-L. Zheng, X.-M. Chen, *Inorg. Chem.* 44 (2005) 4270.
- [34] N.J. Turro, *Modern Molecular Photochemistry*, University Science Books, Sausalito, CA, 1991.
- [35] J.M. Klessinger, J. Michl, *Excited States and Photochemistry of Organic Molecules*, VCH, New York, 1995.
- [36] D.V. Scaltrito, D.W. Thompson, J.A. O'Callaghan, G.J. Meyer, *Coord. Chem. Rev.* 208 (2000) 243.
- [37] S.-L. Zheng, P. Coppens, *Chem. Eur. J.* 11 (2005) 3583.
- [38] S.-L. Zheng, P. Coppens, *Cryst. Growth Des.* 5 (2005) 2050.
- [39] Y.-P. Tong, S.-L. Zheng, X.-M. Chen, *Eur. J. Inorg. Chem.* (2005) 3734.
- [40] Y.-W. Lin, Y.-P. Tong, *Inorg. Chem. Commun.* 12 (2009) 208.
- [41] Y.-P. Tong, Y.-W. Lin, *Inorg. Chim. Acta* 362 (2009) 2033.
- [42] Y.-P. Tong, Y.-W. Lin, *Inorg. Chim. Acta* 362 (2009) 2167.
- [43] S.-L. Zheng, X.-M. Chen, *Aust. J. Chem.* 57 (2004) 703.